Cancer Research

Combined *MYC* Activation and *Pten* Loss Are Sufficient to Create Genomic Instability and Lethal Metastatic Prostate Cancer

Gretchen K. Hubbard[1,2], Laura N. Mutton[1], May Khalili[1], Ryan P. McMullin[1], Jessica L. Hicks[2], Daniella Bianchi-Frias[3], Lucas A. Horn[1], Ibrahim Kulac[2], Michael S. Moubarek[1], Peter S. Nelson[3], Srinivasan Yegnasubramanian[4], Angelo M. De Marzo[2,4,5], and Charles J. Bieberich[1]

Abstract

Genetic instability, a hallmark feature of human cancers including prostatic adenocarcinomas, is considered a driver of metastasis. Somatic copy number alterations (CNA) are found in most aggressive primary human prostate cancers, and the overall number of such changes is increased in metastases. Chromosome 10q23 deletions, encompassing *PTEN*, and amplification of 8q24, harboring *MYC*, are frequently observed, and the presence of both together portends a high risk of prostate cancer-specific mortality. In extant genetically engineered mouse prostate cancer models (GEMM), isolated *MYC* overexpression or targeted *Pten* loss can each produce early prostate adenocarcinomas, but are not sufficient to induce genetic instability or metastases with high penetrance. Although a previous study showed that combining *Pten* loss with focal *MYC* overexpression in a small fraction of prostatic epithelial cells exhibits cooperativity in GEMMs, additional targeted *Tp53* disruption was required for formation of metastases. We hypothesized that driving combined *MYC* overexpression and *Pten* loss using recently characterized *Hoxb13* transcriptional control elements that are active in prostate luminal epithelial cells would induce the development of genomic instability and aggressive disease with metastatic potential. Neoplastic lesions that developed with either *MYC* activation alone (*Hoxb13-MYC*) or *Pten* loss alone (*Hoxb13-Cre* | $Pten^{Fl/Fl}$) failed to progress beyond prostatic intraepithelial neoplasia and did not harbor genomic CNAs. By contrast, mice with both alterations (*Hoxb13-MYC* | *Hoxb13-Cre* | $Pten^{Fl/Fl}$, hereafter, BMPC mice) developed lethal adenocarcinoma with distant metastases and widespread genome CNAs that were independent of forced disruption of *Tp53* and telomere shortening. BMPC cancers lacked neuroendocrine or sarcomatoid differentiation, features uncommon in human disease but common in other models of prostate cancer that metastasize. These data show that combined *MYC* activation and Pten loss driven by the *Hoxb13* regulatory locus synergize to induce genomic instability and aggressive prostate cancer that phenocopies the human disease at the histologic and genomic levels. *Cancer Res; 76(2); 283–92. ©2015 AACR.*

Introduction

Prostate cancer represents a growing problem as populations across the globe are aging and its incidence is linked tightly to age. The lifetime risk of being diagnosed with prostate cancer in the United States is approximately 1 in 6, yet death occurs in approximately 1 in 33 men. Thus, most prostate cancers are not life-threatening. Lethality most often results from metastasis of castration-resistant disease that spreads to lymph nodes, liver, lungs, and bone. Lethal prostate carcinomas tend to have large numbers of genomic alterations, particularly copy-number/structural alterations (1–4), consistent with the hypothesis that widespread genomic instability may be required for lethal disease development (5, 6). The mechanism by which genetic instability drives disease progression is likely due to the development of intratumoral heterogeneity of genetic changes (most of which, in prostate cancer, are copy number changes), which can drive disease progression as a result of an evolutionary process in which variant subclones are selected that have aggressive features (e.g., the ability to form metastatic deposits and to become castration resistant; ref. 7). Therefore, intensive efforts are focused on determining which somatic genome alterations lead to the development of genetic instability, metastasis and castration resistance. The most common genetic alterations include *TMPRSS2-ERG* gene fusions as well as large-scale copy number changes, with recurrent point mutations and small insertions and deletions occurring less frequently (1–3, 8–11). Frequent copy number alterations (CNA) include deletions on chromosome 8p involving *NKX3-1*, amplifications of chromosome 8q24 involving *MYC*,

[1]Department of Biological Sciences, University of Maryland, Baltimore County, Baltimore, Maryland. [2]Department of Pathology, Johns Hopkins University School of Medicine, Baltimore, Maryland. [3]Divisions of Human Biology and Clinical Research, Fred Hutchinson Cancer Research Center, Seattle, Washington. [4]Sidney Kimmel Comprehensive Cancer Center, Johns Hopkins University School of Medicine, Baltimore, Maryland. [5]The Brady Urological Research Institute, Johns Hopkins University School of Medicine, Baltimore, Maryland.

Note: Supplementary data for this article are available at Cancer Research Online (http://cancerres.aacrjournals.org/).

Angelo M. De Marzo and Charles J. Bieberich contributed equally to this article.

Corresponding Author: Charles J. Bieberich, Department of Biological Sciences, University of Maryland, Baltimore County, 1000 Hilltop Circle, Baltimore, MD 21250. Phone: 410-455-3125; Fax: 410-455-3875; E-mail: bieberic@umbc.edu

doi: 10.1158/0008-5472.CAN-14-3280

and deletions of *PTEN* on chromosome 10q23. Gain of *MYC* at 8q24 and loss of *PTEN* are associated with a high Gleason score, disease progression, and poor clinical outcome (1, 3, 12–21). Further, in a recent study by Liu and colleagues (1), gain of *MYC* and loss of *PTEN* as a combination were the only copy number changes that were associated with a markedly elevated risk of prostate cancer–specific mortality independent of other risk factors, raising the hypothesis that *MYC* gain and *PTEN* loss may cooperate to drive genomic instability and lethal disease in human prostate cancer.

Genetically engineered mouse models (GEMM) that phenocopy all stages of prostate cancer, including the development of pre-invasive prostatic intraepithelial neoplasia lesions, locally invasive disease, metastatic dissemination to relevant organs, and the progression to castration resistance in immune-competent animals, would prove invaluable. Despite two decades of effort to develop mouse prostate cancer models, all extant models have at least one of the following limitations: (i) they are driven by alterations in genes not commonly found to be genetically altered in human prostate cancer; (ii) they do not develop widespread metastatic disease; (iii) they develop prominent histologic features not commonly found in human prostate cancer (e.g., small cell neuroendocrine or sarcomatoid differentiation); or (iv) they generally do not develop significant numbers of genomic alterations/genetic instability in the absence of forced telomere dysfunction (22–24). Additionally, as most genetically engineered models of prostate cancer rely on forced androgen-driven oncogene expression, these models are limited when exploring the effects of castration/androgen deprivation, because such treatments necessarily result in direct repression of the transgene, which in turn generally leads to growth suppression (22).

Prior studies using GEMMs have shown that in the mouse prostate, loss of both *Pten* alleles, or activation of *MYC*, can each result in PIN and early invasive carcinoma, with a very low penetrance of metastases (22). Kim and colleagues developed Z-MYC mice, in which a CMV enhancer/β actin promoter–driven *MYC* gene is expressed in a small fraction of luminal cells upon Probasin/Cre–mediated activation (25). The lesions obtained were proliferative but were reported to be histologically normal or arrested at low-grade PIN. Deletion of one or both alleles of *Pten* in Z-MYC mice resulted in acceleration of PIN and early carcinoma development, showing cooperativity between *MYC* and *Pten*, although metastases were not reported (25). In a subsequent study, Z-MYC mice with single copy *Pten* disruption ($Pten^{fl/\pm}$) on a $Tp53^{-/-}$ background resulted in selection for loss of the second *Pten* allele and the development of carcinomas and lymph node metastases (26). These findings further demonstrate cooperativity between *MYC* and *Pten*, although metastases developed only in mice lacking *Tp53*, distant metastases to other sites were not seen, and genomic instability was not examined (26). Cho and colleagues (27) used intraprostatic lentiviral infection to inactivate *Pten* and *Tp53* (RapidCaP) and found that distant metastatic lesions exhibited increased Myc expression, which was required for metastatic tumor formation/maintenance. Further, using a similar strategy to activate MYC in the context of low Pten ($Pten^{hy/-}$), Cho and colleagues demonstrated cooperativity between *MYC* and *Pten* in the development of local disease spread, although distant metastases were not seen (27). To our knowledge, the only study to date to report widespread metastatic prostate carcinoma and genomic instability was in mice with targeted disruption of both copies of *Tp53* and *Pten* in the setting of forced telomere shortening (6). However, aggressive tumors in these mice with telomere dysfunction have been reported to be largely sarcomatoid, a phenotype lacking in the vast majority of human prostatic cancers (22).

In the present work, we show that human *MYC* activation and *Pten* loss driven by androgen-independent *Hoxb13* control elements in mouse prostate luminal cells (28) produces genomic instability and highly penetrant metastatic disease in the absence of induced telomere dysfunction or *Tp53* loss of function. This model, simulating the highly relevant MYC activation and PTEN loss observed in aggressive human cancers, generates prostate adenocarcinomas that recapitulate many key aspects of the human disease, including widespread metastases to multiple organs such as lymph nodes, liver and lung.

Materials and Methods

Generation of *Hoxb13-Cre* and *Hoxb13-MYC* transgenic mice

The Cre recombinase coding sequence was PCR-amplified from pTurboCRE (GenBank accession no. AF334827) with the following primers: forward, 5′-CGCAGATCTGGCACCCAAGAAGAAGAGGAAG-3′; and reverse, 5′-CTGCAAGATGGCGATTAGTCTAGATCTGCG-3′. The resulting PCR product was digested with *Bgl*II and inserted into *BamH*I-digested *pLZURA-Nkx* (29). The SV40 early poly(A) signal present on a 135-bp *Xba*I fragment was inserted downstream of the CRE open reading frame into an *Spe*I site to generate *pNkx-TCRE*. To generate *pHoxb13-TCRE*, a *Sma*I-*Spe*I fragment containing the coding region of CRE was obtained from *pNkx-TCRE* and cloned into *Sma*I- and *Spe*I-digested *pLZKAN-Hoxb13*. A recombinogenic fragment of *pHoxb13-TCRE* was released by *Kpn*I-*Sac*II digestion, purified by sucrose fractionation, and recombineered into exon 1 of the *Hoxb13* transcription unit at codon 8 within BAC RP23-335O22 as described (28). *Escherichia coli* strain DY380 transformants selected for chloramphenicol resistance were confirmed to contain the *Cre* coding region by RFLP analysis. A correctly recombined *Hoxb13-TCRE* BAC clone was prepared using Qiagen Large-Construct DNA preparation reagents according to the manufacturer's instructions, linearized by with PI-*Sce*I digestion, purified on a 10% to 40% sucrose gradient and injected into single-cell FVB/N embryos. Potential transgenic founders were screened by Southern blot analyses of genomic tail DNA digested with *Eco*RI and *Eco*RV. A 255-bp probe within *Hoxb13* exon 1 (+124 to +378 bp) was used for Southern blot analyses. Transgenic founder mice were identified by the presence of a 10-kb hybridizing component. PCR-based genotyping of F_1 offspring of founders bred to FVB mates was performed to amplify a 286-bp fragment within *Cre* with the following primers: forward, 5′-TCGCAAGAACCTGATGGACA-3′; and reverse, 5′-CAGCATTGCTGTCACTTGG-3′. *Hoxb13-Cre* activity was functionally tested using the R26R allele (30). Heterozygous R26R mice (The Jackson Laboratory, Bar Harbor, Maine) were backcrossed to FVB/N and F_1 offspring carrying the R26R locus were identified by Southern blot analyses using a *lacZ* probe on *Eco*RV digested tail DNA. R26R × FVB F_1 mice were interbred to derive an F_2 and homozygous R26R offspring were identified by Southern blot analyses. *Hoxb13-TCRE* founders were bred to homozygous R26R mice and double transgenic mice offspring were identified by PCR and confirmed by Southern blot analyses as described above. The *Hoxb13-MYC* BAC was generated using the same strategy described above for the *Hoxb13-TCRE* BAC. The

human MYC coding sequence was PCR-amplified from pCMV-Sport6 (Open Biosystems) with the following primers: forward, 5′-GCATCCCGGGGATCCACCCCTCAACGTTAGCTTCACC-3′; and reverse, 5′-GCGGATCCACTAGTTCCTTACGCACAAGAGT-TCCGTA-3′. The resulting PCR product was digested with *BamH*I and inserted into a *BamH*I-digested vector bearing *Hoxb13* homologous arms for recombineering. The β-globin intron/poly (A) signal present in the pUGH17-1 vector (31) was PCR amplified and inserted downstream of the MYC open reading to generate *pHoxb13-MYC*-BG poly(A). A recombinogenic fragment of *pHoxb13-MYC*-BG poly(A) (complete sequence available upon request) was released by *Kpn*I *and Nhe*I digestion, purified by sucrose fractionation, and recombineered into exon 1 of the *Hoxb13* transcription unit at codon 8 within BAC RP23-335O22 as described (28). *E. coli* strain DY380 transformants selected for Kanamycin resistance were confirmed to contain the *MYC* coding region by RFLP analysis. A correctly recombined *Hoxb13-MYC*-BG Poly(A) BAC clone was prepared using Qiagen (Valencia) Large-Construct DNA preparation reagents according to the manufacturer's instructions, linearized by with PI-*Sce*I digestion, purified on a 10% to 40% sucrose gradient and injected into single-cell FVB/N embryos. Potential transgenic founders were screened by Southern blot analyses of genomic tail DNA digested with *Eco*RI. A 255-bp probe within *Hoxb13* exon 1 (+124 to +378 bp) was used for Southern blot analyses. Transgenic founder mice were identified by the presence of a 6-kb hybridizing component. PCR-based genotyping of F_1 offspring of founders bred to FVB mates was performed to amplify a 238-bp fragment within *MYC* with the following primers: forward, 5′-TCCAGCGCCTTCTCTC-CGTCCTCGGATTCTC-3′; reverse, 5′-ATGCGTCGACCCTTTTGC-CAGGAGCCTGCCTCTTTTCCAC-3′.

Conditional *Pten* knockout mice

Mice carrying a floxed Pten ($Pten^{Fl}$) conditional allele (32) were purchased from The Jackson Laboratory (stock number 004597). The deletion of *Pten* allele(s) was confirmed using the following primers, which yielded a wild-type product of 240 bp and a floxed allele product of 320 bp: forward primer 1, 5′-TTGCACAG-TATCCTTTTGAAG-3′; forward primer 2, 5′-GTCTCTGGTCCTTAC TTCC-3′; and reverse primer, 5′-ACGAGACTAGTGAGACGTGC-3′. The PCR protocol was followed according to the NCI Mouse Repository.

Mating scheme

Hemizygous *Hoxb13-Cre*$^{+/-}$ mice were mated to the $Pten^{Fl/Fl}$ mice to generate the genotype *Hoxb13-Cre*$^{+/-}$ | $Pten^{Fl/+}$. These mice were interbred to generate mice with the *Hoxb13-Cre*$^{+/-}$ | $Pten^{Fl/Fl}$ genotype. *Hoxb13-MYC* mice were then mated to *Hoxb13-Cre*$^{+/-}$ | $Pten^{Fl/Fl}$ mice to generate offspring heterozygous for all three alleles (*Hoxb13-MYC*$^{+/-}$ | *Hoxb13-Cre*$^{+/-}$ | $Pten^{Fl/+}$). These mice were then interbred to generate triple transgenic mice, which were *Hoxb13-MYC*$^{+/-}$ | *Hoxb13-Cre*$^{+/-}$ | $Pten^{Fl/Fl}$, referred to as BMPC mice in this article. Cohorts of triple transgenic males for analyses were derived from crosses of varying genotypes, including *Hoxb13-MYC*$^{+/-}$ | *Hoxb13-Cre*$^{+/-}$ | $Pten^{Fl/+}$ males mated with *Hoxb13-MYC*$^{+/-}$ | *Hoxb13-Cre*$^{+/-}$ | $Pten^{Fl/Fl}$ females, in addition to *Hoxb13-MYC*$^{+/-}$ | *Hoxb13-Cre*$^{+/-}$ | $Pten^{Fl/Fl}$ by *Hoxb13-MYC*$^{+/-}$ | *Hoxb13-Cre*$^{+/-}$ | $Pten^{Fl/Fl}$ crosses.

Tissue analysis

Control and tumor tissues were dissected and fixed in 10% neutral-buffered formalin for 48 hours at room temperature and then transferred to phosphate buffered saline at 4°C until submission. Samples were processed, paraffin-embedded, sectioned, and stained with hematoxylin and eosin (H&E) according to standard protocols. Immunohistochemical analysis was performed on tissue sections using antibodies that include MYC (Rabbit Monoclonal, Clone EP121, Epitomics, 1:600), Pten (Rabbit Monoclonal, Clone D4.3, Cell Signaling Technology, 1:200), Ki67 (Rabbit Polyclonal, NCL-Ki67p, Leica Biosystems, 1:3,000), Nkx3.1 (Rabbit Polyclonal, 1:6,000; ref. 33), cytokeratin 18 (CK18; Rabbit Polyclonal, Novus Biologicals, NB100-91814, 1:8,000), androgen receptor (AR; Rabbit Polyclonal, Santa Cruz Biotechnology, sc-816, 1:400), chromogranin A (Rabbit Polyclonal, Novus Biologicals, NB120-15160, 1:8,000), FoxA1 (Rabbit Polyclonal, Santa Cruz, sc-6553, HNF-3 α/β, 1:400), FoxA2 (Rabbit Polyclonal, Abcam, HNF-3 Beta, 1:400), p63 (Mouse Monoclonal, Clone 4A4, Neomarkers, 1:600), p-AKT (Rabbit Monoclonal, Cell Signaling Technology, Ser473 D9E, 1:100), and p-S6 (Rabbit Monoclonal, Cell Signaling Technology, Ser235/236 D57.2.2E; 1:4,000).

Array CGH copy number analysis and associated bioinformatics

For four BMPC mice, tail, primary prostate cancer, and metastatic tumor tissues were obtained and DNA was extracted using the Qiagen AllPrep DNA/RNA/Protein Mini Kit. Mouse male reference DNA (The Jackson Laboratory) was used as a common reference for all samples. Similarly, tail and prostate DNA were prepared from three *Hoxb13-MYC*$^{+/-}$ and three *Hoxb13-Cre*$^{+/-}$ | $Pten^{Fl/Fl}$ mice. For *Hoxb13-MYC*$^{+/-}$ mice, the ventral lobes, which develop the most extensive PIN lesions, were used from mice that were between 10 and 13 weeks of age and similarly for the *Hoxb13-Cre*$^{+/-}$ | $Pten^{Fl/Fl}$ mice, the anterior lobe was used from mice that were between 17 and 20 weeks of age. Array comparative genomic hybridization (aCGH) was performed with SurePrint G3 Mouse CGH 4 × 180 K Microarrays essentially as recommended by the manufacturer (Agilent Technologies). Briefly, 1.5 μg of genomic DNA was digested for 2 hours at 37°C with 1 unit/mL of AluI and RsaI restriction endonucleases (Invitrogen). The reaction was terminated by incubating at 65°C for 20 minutes. Digested DNA was subsequently labeled with Cy3 dye (for experimental samples: tail DNA, primary prostate cancer DNA, or metastatic prostate cancer DNA samples) or with Cy5 for the reference male DNA. Each Cy3-labeled sample was combined with the Cy5-labeled reference DNA and diluted in aCGH buffer and mouse Cot-1 DNA (Invitrogen). These combined labeled DNA samples were hybridized on the Mouse CGH 4 × 180 K microarrays in a hybridization rotator at 20 rpm for 40 hours at 65°C before being washed in Oligo aCGH Wash buffers according to the manufacturer's instructions (Agilent). aCGH slides were scanned on an Agilent DNA Microarray Scanner at a resolution of 2 μm. The resulting Agilent Feature Extraction data were analyzed using the Partek Genomics Suite v. 6.6 software (Partek). The Cy5/Cy3 log-ratio data were imported from the feature extraction file, transformed to log base 2 and multiplied by −1 to generate log2ratio(Cy3/Cy5). To facilitate identification of somatic CNAs in the cancer DNA not present in the tail DNA, the logratio data from the tail DNA for each mouse were subtracted from the matched primary and metastatic cancer logratio data. The resulting baseline subtracted logratio data were subjected to copy number detection using the genomic segmentation pipeline under default settings. All significantly altered regions with a false

discovery rate of 0.05 were identified for each sample. The Partek copy number pipeline was used under default conditions to summarize regions of CNAs across samples, annotate with overlapping genes, and carry out gene ontology gene set enrichment analysis on genes overlapping with regions showing gains or losses in any sample. Enriched gene ontology terms with FDR = 0.05 were identified.

Results

FVB/N mice carrying a recombineered transgene (34), allowing *Hoxb13*-driven *MYC* overexpression in the prostate epithelium (*Hoxb13-MYC* mice), developed PIN lesions that were characterized by marked nuclear and nucleolar enlargement within cells that maintained a columnar cellular polarity (Supplementary Fig. S1), similar to changes seen in Hi-MYC and Lo-MYC mice and to changes seen in human high-grade PIN (35, 36). MYC overexpression was observed in luminal epithelial cell nuclei (Supplementary Fig. S2C). Further phenotypic analyses showed robust androgen receptor (AR) and keratin 18 expression (CK18) in the atypical luminal cells, and positive Pten staining in all epithelial cells (Supplementary Fig. S2). To disrupt *Pten* alleles within the prostate, $Pten^{Fl\,|\,Fl}$ mice (The Jackson Laboratory; ref. 37) were crossed to FVB/N transgenic mice with *Hoxb13*-driven Cre recombinase expression (*Hoxb13-Cre* | $Pten^{Fl/Fl}$ mice). Prostate lobes of *Hoxb13-MYC* and *Hoxb13-Cre* | $Pten^{Fl/Fl}$ were dissected at multiple time points and only PIN lesions, with no invasive carcinomas, were present up to one year of age.

We next generated compound mutant mice with *Hoxb13*-driven overexpression of *MYC* and with *Hoxb13*-mediated conditional disruption of *Pten* alleles (*Hoxb13-MYC*$^{+}$ | *Hoxb13-Cre*$^{+}$ | $Pten^{Fl/Fl}$), referred to as BMPC mice. Cohorts of BMPC males were necropsied at various intervals from 4 weeks onward (Supplementary Tables S1 and S2). For controls, *Hoxb13-MYC*$^{+}$ | *Hoxb13-Cre*$^{+}$ | $Pten^{FL/+}$ males as well as wild-type FVB/N males were used. All BMPC mice developed PIN lesions in all four prostate lobes by 4 to 8 weeks. Immunohistochemical analysis confirmed overexpression of MYC and variable loss of Pten in PIN cells, which also phenocopied human PIN for strong positive staining for AR and Foxa1, with variable loss of Nkx3.1 (Fig. 1 and Supplementary Figs. S3 and S4). MYC staining occurred in virtually all cells that showed morphologic PIN by H&E staining, yet Pten loss appeared quite heterogeneous (Fig. 1C, Supplementary Fig. S4), despite Cre expression being driven by the same *Hoxb13* regulatory elements. This focal loss of Pten is reminiscent of human prostate cancer in that primary tumors often lose PTEN as a subclonal process subsequent to *TMPRSS2-ERG* gene fusion events (38). Increased staining for p-AKT and p-S6 ribosomal protein was evident in areas of Pten loss (Supplementary Fig. S4) in PIN

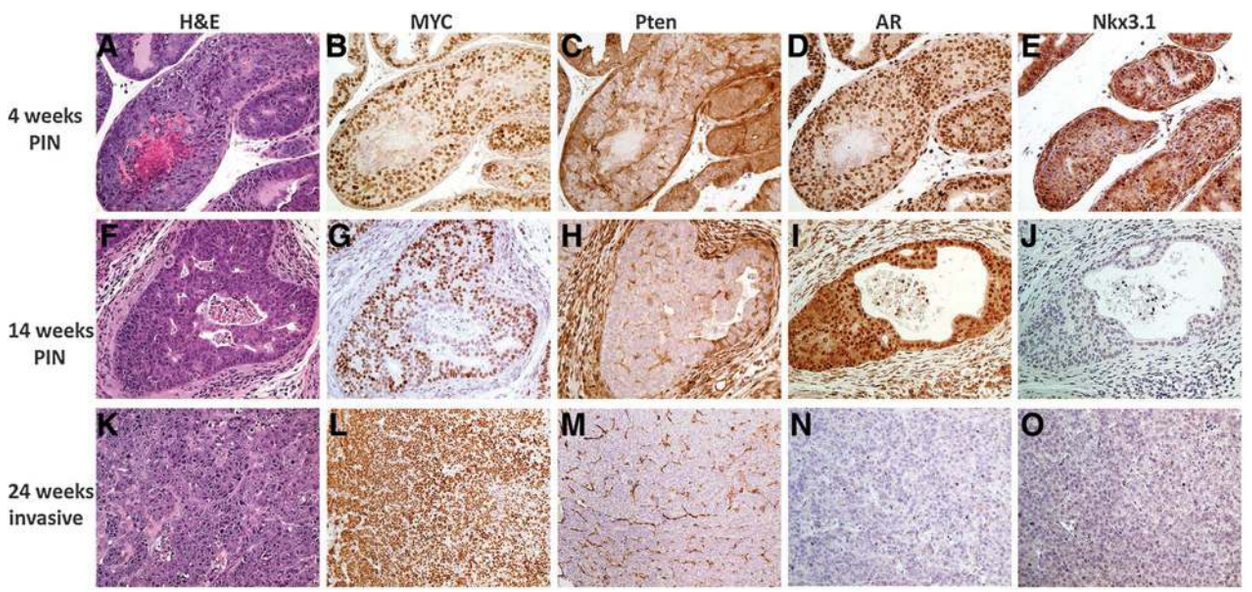

Figure 1.
Morphology and phenotype of PIN lesions (ventral lobe shown here) and primary tumors in BMPC mice. Cohorts of BMPC males were necropsied at various intervals. By 4 weeks of age CribPIN/CIS (corresponding to high-grade PIN or mPIN 4), lesions were observed in all prostate lobes ($n = 3$ of three mice at each time point). PIN lesions were characterized by marked nuclear and nucleolar enlargement and overall loss of cell polarity that generally filled most or all of the lumens with cribriform or solid structures, at times with central necrosis (H&E-stained lesions in A and F). PIN lesions were most prevalent and extensive in the ventral lobe and anterior lobes as compared with the dorsal and lateral lobes. IHC staining revealed robust MYC nuclear staining in all PIN (B and G) lesions and heterogeneous loss of Pten (C and H). PIN cells within prostatic ducts in these compound mutant mice had more severe nuclear pleomorphism than mice overexpressing MYC alone and much more than mice with Pten loss alone. AR protein expression was robust in all PIN acini (D and I), and downregulation of the tumor suppressor Nkx3.1 was evident to varying degrees; reduction (E), and near total loss of Nkx3.1 (J). By 14 weeks, the extent of involvement of all lobes by CribPIN/CIS increased, and stromal thickening as well as chronic inflammation were apparent (F–J). At 14 weeks, overexpression of MYC and loss of Pten by IHC was similar to that seen at 4 weeks, although there was a progressive increase in the neoplastic PIN cells that lacked Pten staining. AR expression began to show variable diminution in intensity seen starting by 14 weeks (I) and was lost by 16 weeks and after (N). Overtly invasive adenocarcinoma lesions (K–O) showed more marked nuclear pleomorphism and nucleolar enlargement than preinvasive lesions. Invasive lesions retained high levels of MYC expression (L) and were completely negative for Pten (M; tumor cells are negative and intervening stromal cells are strongly positive), AR (N), and Nkx3.1 (O). Original magnification, ×200 (A–K, N, O); ×100 (L, M).

lesions and this pattern was similar in large invasive and metastatic lesions (not shown). Stromal invasion was first evident at 12–14 weeks (Supplementary Fig. S5) and as early as 16 weeks, large invasive adenocarcinoma lesions involving multiple prostate lobes were present (Fig. 2). Tumor cells in invasive lesions contained markedly enlarged nucleoli and nuclei (unlike small cell neuroendocrine carcinomas) and showed more pleomorphism than their intraepithelial counterparts (Figs. 1K and 3A, a, e). Although there was occasional acinar/glandular formation, these tumors generally resembled very high-grade primary prostatic adenocarcinomas in humans (Gleason score 5 + 5 = 10). Also like their human counterparts, invasive prostatic carcinomas lacked basal cells as shown by the absence of staining for p63 and keratin 5 (CK5; not shown). Further, invasive carcinomas remained positive for CK18 and FoxA1 (not shown), but were either negative for neuroendocrine markers (chromogranin A, FoxA2) or showed only variable, occasional tumor cell staining (<1%; Supplementary Fig. S6). All overtly invasive lesions, typically showing very high volume disease, were negative for AR (Fig. 1N). Among animals 16 weeks of age or older, 97% (31/32) developed gross metastases to pelvic lymph nodes (Fig. 2A). Grossly visible and microscopic metastases were also common to liver (Fig. 3A, a–d), and lung, and one mouse had a single bone metastasis in a thoracic vertebra (Fig. 3A, e–h; Supplementary Table S2). Tumor cells within metastatic lesions were similar to invasive primary lesions in that they were strongly positive for MYC (Fig. 3A, c and g), completely negative for Pten protein (Fig. 3A, d and h), positive for CK18 (Fig. 3A, b and f) and Foxa1 (not shown), and negative or focally positive for neuroendocrine markers including chromagranin A, and Foxa2 (Supplementary Fig. S6). They were also negative for nuclear AR and basal cell markers (CK5 and p63; data not shown). All BMPC mice ($N = 32$) reached criteria for euthanasia by 40 weeks (Fig. 3B). By contrast, none of the control *Hoxb13-MYC*$^{+}$ | *Hoxb13-Cre*$^{+}$ | *Pten*$^{FL/+}$ mice developed large primary invasive adenocarcinomas or metastatic lesions (Supplementary Table S3) by 52 weeks of age, indicating that complete Pten loss was required for the development of aggressive/lethal carcinomas. No sarcomatoid or neuroendocrine differentiation was observed in either primary or metastatic lesions.

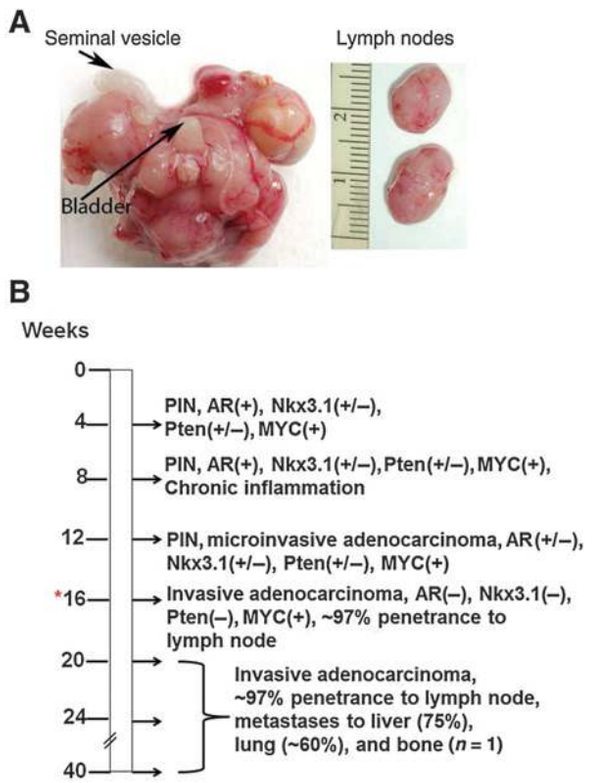

Figure 2.
Gross anatomy of tumors and timeline of disease in BMPC mice. A, gross appearance of primary prostatic tumor and pelvic lymph node metastasis from a BMPC mouse at 24 weeks of age. Note that primary tumor is encasing much of the genitourinary tract, although primary tumors generally did not invade directly through the bladder wall and never invaded into the rectum. Ruler is in centimeters. B, overall timeline and phenotypic features of BMPC mice.

To determine the effects of androgen deprivation, we castrated animals at different time points. Castration at 4 weeks of age led to a marked delay in the development of aggressive cancers, demonstrating the early androgen dependence of disease (Supplementary Table S4; Supplementary Fig. S7). Nevertheless, histologic analyses revealed residual PIN at times, and, in one case, a microscopic invasive carcinoma at 38 weeks of age, suggesting that these castration-resistant residual lesions have potential to progress, albeit at a markedly reduced rate. Castration at either 8 or 14 weeks also had a marked effect by delaying tumor progression, especially metastases (Supplementary Table S4). Nevertheless, lesions often progressed to invasive disease, with occasional metastatic spread, indicating the spontaneous emergence of castration-resistant disease (Supplementary Table S4).

We performed genome-wide microarray-based comparative genomic hybridization (aCGH) analyses on DNA from matched frozen primary tumor tissue, one site of metastasis (either lymph node or lung), and tail (germline) DNA from each of four mice. Every primary and metastatic tumor analyzed showed evidence of significant somatic CNAs, with each tumor harboring on average approximately 20 regions of copy number gains or losses spanning significant portions of the genome (range: 7–43 regions, spanning 1.27–118.95 Mbp of sequence; Supplementary Tables S6 and S7; Fig. 4). Among these alterations, 10 regions showed evidence of recurrent somatic CNAs, occurring in at least 1 tumor from at least 2 BMPC mice (Fig. 4A, Supplementary Table S8), and 8 regions showed evidence of high copy number gain (logratio > 1.2; 3 regions) or low copy number loss representing putative homozygous loss (logratio < −1.2; 5 regions; Supplementary Table S9). Interestingly, genes within regions of copy number gain were enriched for chromatin modulation and hormone signaling pathways, whereas genes within regions of copy number loss were enriched for cytokine/chemokine signaling, immune system, and development/differentiation pathways (Supplementary Fig. S7); these pathway categories are often altered at a genetic or epigenetic level in human prostate cancers (2, 39). Representative CNAs from chromosome 8, including a large deletion encompassing a smaller region of putative homozygous loss in both the primary and metastasis lesions from one mouse, is shown in Fig. 4B. Clustering of copy number data revealed that primary and metastatic tumors from the same mouse were more similar to each other than they were to tumors from other mice (Fig. 4B, dendrogram), suggesting that the primary and metastatic lesions within mice had clonal evolutionary relationships, similar to those observed for human prostate cancer (39–41). In contrast,

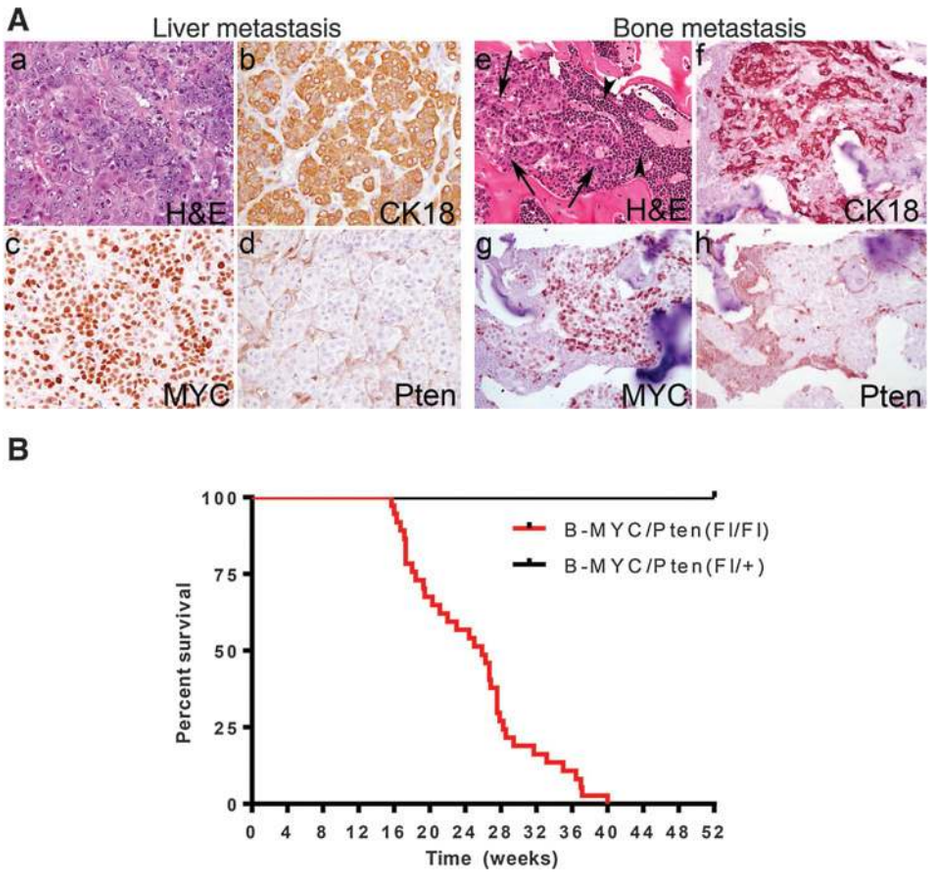

Figure 3.
MYC expression combined with Pten loss leads to metastatic adenocarcinomas and markedly reduced survival. A, morphology and phenotype of metastatic lesions in BMPC mice. Note abundant cytoplasm and enlarged prominent nucleoli in tumor cells in the liver. Also note strong positive staining for cytokeratin and MYC in the liver (c) and bone metastasis (g) and complete absence of Pten staining in tumor cells (d and h). e, arrows indicate tumor cells in bone and arrowheads indicate resident bone marrow cells. Original magnifications, ×200 (a–d) and ×100 (e–h). B, survival curve showing the aggressive nature of the combination of MYC overexpression and Pten loss in the BMPC mice.

CNA analyses of *Hoxb13-MYC*$^{+/-}$ and *Hoxb13-Cre*$^{+/-}$ | *Pten*$^{Fl/Fl}$ mice with PIN lesions revealed no CNAs. No correlations were identified between the number of CNAs and the extent or location of metastases.

Although late-stage human prostate adenocarcinomas frequently show loss of heterozygosity at the *TP53* locus, copy number variation at the mouse *Tp53* locus was not observed in BMPC tumors. To explore the possibility that point mutation of the *Tp53* gene may have occurred, exons 3 to 8 (data not shown) were PCR-amplified and sequenced from tumor DNA extracted from the same cases. No mutations were observed.

Discussion

Here we show that conditional activation of *MYC* along with loss of Pten in mouse prostatic luminal epithelial cells, simulating the genetic activation of *MYC* and loss of *PTEN* observed in aggressive human prostate cancers, creates the full spectrum of prostate cancer initiation and progression in a manner that strongly phenocopies human prostate cancer. This disease progression appears to occur through the induction of genomic instability evidenced by widespread CNAs, similar to human prostate cancer progression. Thus, although activation of *MYC* alone or disruption of *Pten* alone result in very early disease, the combination of these two events synergize in creating profound changes leading to highly aggressive disease that progresses from PIN precursor lesions, to invasive adenocarcinoma, to metastatic adenocarcinoma, and ultimately to castration-resistant metastatic adenocarcinoma. As these primary tumors develop highly prevalent CNAs, and neither alteration alone results in significant numbers of CNAs (24, 35), we show the first evidence *in vivo* that the combination of *Pten* loss and *MYC* activation in prostatic luminal cells is sufficient to induce the acquisition and tolerance of genetic instability, independent of forced telomere dysfunction or loss/mutation of Tp53. MYC overexpression is known to induce genetic instability (42), and our results suggest that PTEN serves to repress this process in prostate cells. Recent findings indicating that PTEN is required for DNA repair and that loss of PTEN can result in high levels of DNA damage in cells that simultaneously repress apoptosis due to increased PI3K signaling, are consistent with this hypothesis (43). Future studies are required to address this question directly. It is interesting to note that a subset of the CNAs detected in the BMPC tumors overlap with regions of known copy number variants in mouse strains. These alterations are likely to be additional somatic alterations at these regions even beyond the baseline CNV state in the mouse strain, since we controlled for the constitutional copy number state with the tail DNA. In addition, the single gene models did not show these similar CNAs, suggesting that these regions were not simply identified due to undercorrection.

Several previous attempts have been made to model *Pten* loss or PI3K pathway activation in combination with *MYC* overexpression. Prostate-epithelial restricted co-expression of human *AKT1* and *MYC* leads to accelerated disease progression, stromal

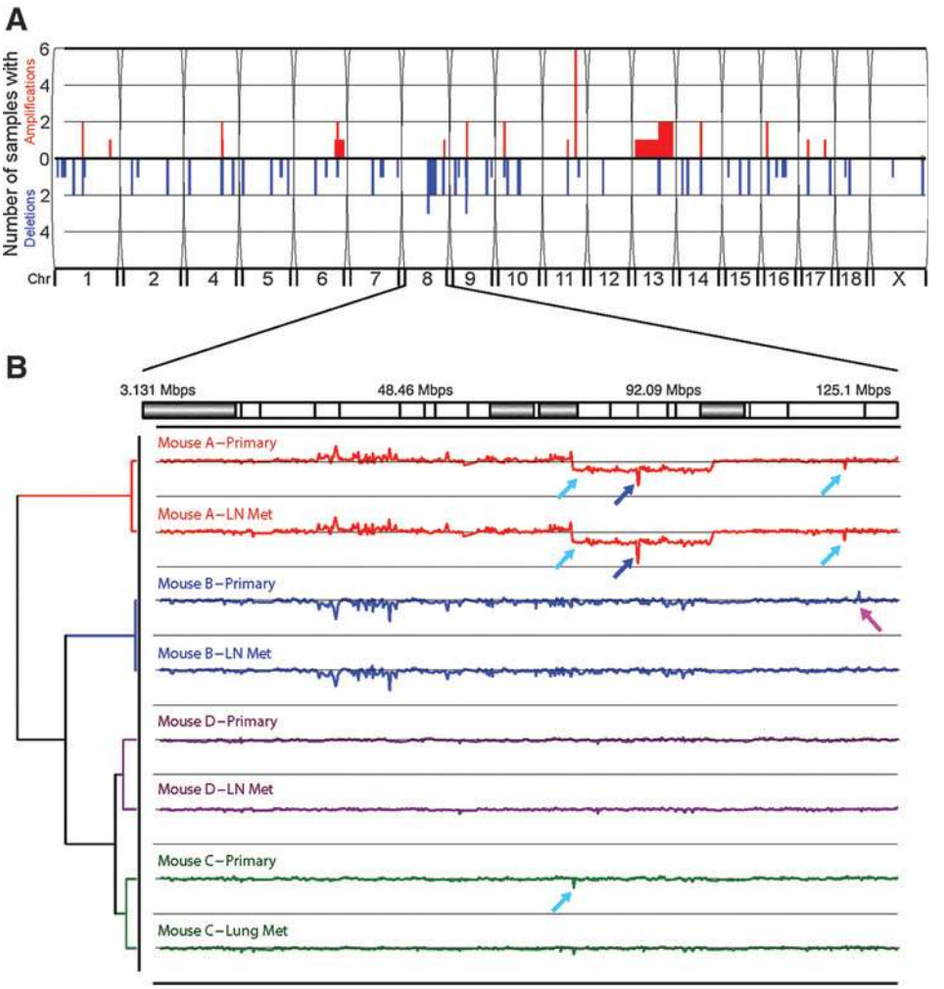

Figure 4.
Primary and metastatic prostate cancer lesions from BMPC mice can develop large-scale somatic CNAs. A, histogram showing number of cancer lesions harboring the indicated regions of somatic copy number gains and losses. Red regions, gains; blue regions, losses. B, a magnified view of representative somatic CNAs within chromosome 8. Top, the chromosomal ideogram. For each mouse, the smoothed copy number logratio is plotted across the chromosome. Light blue arrows, regions of statistically significant single copy number loss determined. Dark blue arrows, regions of high copy number loss with logratio <−1.2, likely representing homozygous deletion. Purple arrow, a region of statistically significant amplification. The dendrogram shows results of unsupervised hierarchical clustering of the copy number data.

changes, and immune cell infiltration but does not affect metastasis (44). In addition, conditional *Pten* loss in the Hi-MYC background gave rise to large primary tumors (44), although metastatic lesions were not reported upon. Highly focal epithelial *MYC* expression (Z-MYC mice) combined with conditional *Pten* loss also fostered the appearance of more aggressive pathology with increased proliferation and development of early invasive carcinomas apparently without affecting metastasis (25, 26). When combined with loss of one allele of *Tp53*, Z-MYC/Pten mice developed adenocarcinoma that metastasized to lymph nodes (26). Given the well-documented dose-dependent biologic effects of MYC overexpression (45), we submit that the lethal phenotype that invariably develops in the BMPC mice is likely a consequence of a higher level or broader expression of MYC throughout the prostatic epithelium driven by *Hoxb13* regulatory elements in our system, at least as compared with the Z-MYC model. Interestingly, Kim and colleagues (25) speculated that increased MYC expression could lead to genetic instability, and the data reported here provide evidence that this is indeed the case.

It is of interest that other studies that have obtained macroscopic metastatic disease in mice by disruption of both copies of *Pten* have reported that disease progression required loss of both copies of *Tp53* (27, 46). Thus, the current study, in which we used mice that were wild type for *Tp53* and found no evidence of *Tp53* alterations in aggressive lesions from BMPC mice, demonstrates the novel finding that in the setting of *MYC* overexpression and *Pten* loss, emergence of aggressive distant metastatic disease can occur without *Tp53* loss.

Invasive and metastatic lesions in BMPC mice do not express AR, yet also do not develop neuroendocrine nor sarcomatoid differentiation. Logothetis and colleagues have described highly aggressive prostate cancers that lack AR both with and without overt neuroendocrine features (47), and it is expected that these phenotypes will increase as androgen suppression/AR inhibitor therapies continue to improve and are used in combination. Thus, in addition to providing a model to test novel therapeutics, including those based on immunotherapies, the BMPC model provides a robust system to dissect the molecular bases underlying the evolution of AR-loss in non-neuroendocrine tumors, as well as AR-independent mechanisms of disease progression and growth.

Although the AR-negative phenotype of advanced cancers in BMPC mice does not reflect the AR status of the majority of late-stage human cancers, it is also not completely unexpected. It is well established that conditional loss of *Pten* in the mouse prostate impairs mouse AR (mAR) signaling in the cancers that develop (48). Reduced mAR expression at both the mRNA and

protein levels has been reported, and this diminution can be partially reversed by PI3K pathway inhibition (49). Given that mAR is known to be positively autoregulated in the mouse prostate, the reduction of AR is not, *a priori*, surprising (50). In human prostate cancer cases with *PTEN* loss, human AR (hAR) expression typically persists. Although some *in vitro* evidence suggests that *PTEN* loss may lead to AR stabilization or transcriptional activation (51, 52), transcriptomic analyses of prostate cancer cases clearly demonstrate that androgen-responsive gene signaling is profoundly diminished when *PTEN* is lost (48, 49). We speculate that the differences in AR expression in mice versus human prostate epithelial cells in the context of *PTEN* loss may be related to evolutionary divergence in the extent of *AR* gene autoregulation between primates and rodents. The mAR gene may require a higher degree of autostimulation to maintain transcriptional activity than hAR and results in a threshold-based on/off switch that follows second order kinetics. In contrast, the *hAR* gene may respond in a linear fashion, wherein a reduction in autostimulation would result in reduced transcriptional output but not extinction of expression. Metastatic lesions obtained in RapidCaP mice also do not express AR (27).

The strong parallels with the spectrum of human prostate cancer initiation and progression in this model are likely a result of several important design features in the model. First, this genetically engineered model is driven by concurrent activation of *MYC* and loss of *Pten*, the combination of which has been strongly associated with human prostate cancer aggressiveness (1). Second, *MYC* activation and *Pten* loss were driven by *Hoxb13* regulatory elements, allowing AR-independent genetic modulation. Avoidance of AR-dependent control elements (e.g., the commonly used *probasin* or the derivative ARR2 elements) likely allowed development of castration-resistant disease. In humans, the *HOXB13G84E* allele has recently been demonstrated to be highly associated with increased prostate cancer risk (53–55). Given this, it seems likely that it is expressed in a population of cells that contribute directly to disease development. In mice, *Hoxb13* transcriptional activity is present broadly within the secretory epithelium and in a subset of basal cells in all prostate lobes (28). Interestingly, the tumors that developed in the BMPC animals had a luminal phenotype and loss of Pten was confined to luminal cells in PIN lesions (Supplementary Fig. S3), analogous to human disease. Another potential advantage of the *Hoxb13* regulatory elements for driving prostate expression of MYC and loss of Pten is that we have not observed any leakiness of expression of *Hoxb13*-based reporter genes, MYC overexpression or Pten loss in any of these animals, whereas leakiness of the rat probasin promoter into stromal elements has been observed (56). This feature should facilitate the study of relevant cancer–stromal interactions because the genetic modulations would not occur in the stromal cells of the BMPC model. These design features have allowed us to avoid the pitfalls of other recently developed prostate cancer GEMMs, including the common occurrence of sarcomatoid or overt neuroendocrine differentiation, lack of progression through early and advanced stages of human prostate cancer in tractable time scales, and/or lack of development of genetic instability (22, 57, 58). These features should facilitate the use of this model to study prostate cancer initiation and disease progression, study mechanisms underlying the cooperativity and synergy of MYC activation and PTEN loss in the development of genomic instability and aggressive human prostate cancers, and test relevant prostate cancer therapeutic strategies in an immunocompetent model.

Disclosure of Potential Conflicts of Interest

No potential conflicts of interest were disclosed.

Authors' Contributions

Conception and design: G.K. Hubbard, M. Khalili, R.P. McMullin, P.S. Nelson, S. Yegnasubramanian, A.M. De Marzo, C.J. Bieberich

Development of methodology: G.K. Hubbard, L.N. Mutton, M. Khalili, R.P. McMullin, L.A. Horn, S. Yegnasubramanian, C.J. Bieberich

Acquisition of data (provided animals, acquired and managed patients, provided facilities, etc.): G.K. Hubbard, L.N. Mutton, M. Khalili, D. Bianchi-Frias, L.A. Horn, I. Kulac, M.S. Moubarek, P.S. Nelson, A.M. De Marzo, C.J. Bieberich

Analysis and interpretation of data (e.g., statistical analysis, biostatistics, computational analysis): G.K. Hubbard, M. Khalili, D. Bianchi-Frias, L.A. Horn, P.S. Nelson, S. Yegnasubramanian, A.M. De Marzo, C.J. Bieberich

Writing, review, and/or revision of the manuscript: G.K. Hubbard, P.S. Nelson, S. Yegnasubramanian, A.M. De Marzo, C.J. Bieberich

Administrative, technical, or material support (i.e., reporting or organizing data, constructing databases): G.K. Hubbard, L.N. Mutton, R.P. McMullin, M.S. Moubarek, S. Yegnasubramanian

Study supervision: G.K. Hubbard, A.M. De Marzo, C.J. Bieberich

Grant Support

This work was supported by the following grants: DAMD17-98-1-8477 and R21CA105342 to C.J. Bieberich; a Patrick C. Walsh Prostate Cancer Research Fund award to A.M. De Marzo and C.J. Bieberich; a 2013 Movember-Prostate Cancer Foundation Challenge Award to A.M. De Marzo, S. Yegnasubramanian, and C.J. Bieberich. A PCF Challenge Grant, R01CA183965 and P30CA006973 (NIH/NCI), and a Commonwealth Foundation Grant to S. Yegnasubramanian.

The costs of publication of this article were defrayed in part by the payment of page charges. This article must therefore be hereby marked *advertisement* in accordance with 18 U.S.C. Section 1734 solely to indicate this fact.

Received November 5, 2014; revised September 5, 2015; accepted October 14, 2015; published OnlineFirst November 10, 2015.

References

1. Liu W, Xie CC, Thomas CY, Kim ST, Lindberg J, Egevad L, et al. Genetic markers associated with early cancer-specific mortality following prostatectomy. Cancer 2013;119:2405–12.
2. Taylor BS, Schultz N, Hieronymus H, Gopalan A, Xiao Y, Carver BS, et al. Integrative genomic profiling of human prostate cancer. Cancer Cell 2010;18:11–22.
3. Sun J, Liu W, Adams TS, Sun J, Li X, Turner AR, et al. DNA copy number alterations in prostate cancers: a combined analysis of published CGH studies. Prostate 2007;67:692–700.
4. Hieronymus H, Schultz N, Gopalan A, Carver BS, Chang MT, Xiao Y, et al. Copy number alteration burden predicts prostate cancer relapse. Proc Natl Acad Sci U S A 2014;111:11139–44.
5. Lengauer C, Kinzler KW, Vogelstein B. Genetic instabilities in human cancers. Nature 1998;396:643–9.
6. Ding Z, Wu CJ, Jaskelioff M, Ivanova E, Kost-Alimova M, Protopopov A, et al. Telomerase reactivation following telomere dysfunction yields murine prostate tumors with bone metastases. Cell 2012;148:896–907.
7. Swanton C. Cancer evolution: the final frontier of precision medicine? Ann Oncol 2014;25:549–51.
8. Baca SC, Prandi D, Lawrence MS, Mosquera JM, Romanel A, Drier Y, et al. Punctuated evolution of prostate cancer genomes. Cell 2013;153:666–77.
9. Grasso CS, Wu YM, Robinson DR, Cao X, Dhanasekaran SM, Khan AP, et al. The mutational landscape of lethal castration-resistant prostate cancer. Nature 2012;487:239–43.

10. Tomlins SA, Laxman B, Dhanasekaran SM, Helgeson BE, Cao X, Morris DS, et al. Distinct classes of chromosomal rearrangements create oncogenic ETS gene fusions in prostate cancer. Nature 2007;448:595–9.
11. Rubin MA, Maher CA, Chinnaiyan AM. Common gene rearrangements in prostate cancer. J Clin Oncol 2011;29:3659–68.
12. Visakorpi T, Kallioniemi AH, Syvanen AC, Hyytinen ER, Karhu R, Tammela T, et al. Genetic changes in primary and recurrent prostate cancer by comparative genomic hybridization. Cancer Res 1995;55:342–7.
13. Jenkins RB, Qian J, Lieber MM, Bostwick DG. Detection of c-myc oncogene amplification and chromosomal anomalies in metastatic prostatic carcinoma by fluorescence in situ hybridization. Cancer Res 1997;57:524–31.
14. Wang SI, Parsons R, Ittmann M. Homozygous deletion of the PTEN tumor suppressor gene in a subset of prostate adenocarcinomas. Clin Cancer Res 1998;4:811–5.
15. Yoshimoto M, Cunha IW, Coudry RA, Fonseca FP, Torres CH, Soares FA, et al. FISH analysis of 107 prostate cancers shows that PTEN genomic deletion is associated with poor clinical outcome. Br J Cancer 2007;97: 678–85.
16. Ribeiro FR, Henrique R, Martins AT, Jeronimo C, Teixeira MR. Relative copy number gain of MYC in diagnostic needle biopsies is an independent prognostic factor for prostate cancer patients. Eur Urol 2007;52:116–25.
17. Lotan TL, Gurel B, Sutcliffe S, Esopi D, Liu W, Xu J, et al. PTEN protein loss by immunostaining: analytic validation and prognostic indicator for a high risk surgical cohort of prostate cancer patients. Clin Cancer Res 2011; 17:6563–73.
18. Krohn A, Diedler T, Burkhardt L, Mayer PS, De Silva C, Meyer-Kornblum M, et al. Genomic deletion of PTEN is associated with tumor progression and early PSA recurrence in ERG fusion-positive and fusion-negative prostate cancer. Am J Pathol 2012;181:401–12.
19. Cuzick J, Yang ZH, Fisher G, Tikishvili E, Stone S, Lanchbury JS, et al. Prognostic value of PTEN loss in men with conservatively managed localised prostate cancer. Br J Cancer 2013;108:2582–9.
20. Barros-Silva JD, Ribeiro FR, Rodrigues A, Cruz R, Martins AT, Jeronimo C, et al. Relative 8q gain predicts disease-specific survival irrespective of the TMPRSS2-ERG fusion status in diagnostic biopsies of prostate cancer. Genes Chromosomes Cancer 2011;50:662–71.
21. Leversha MA, Han J, Asgari Z, Danila DC, Lin O, Gonzalez-Espinoza R, et al. Fluorescence in situ hybridization analysis of circulating tumor cells in metastatic prostate cancer. Clin Cancer Res 2009;15:2091–7.
22. Ittmann M, Huang J, Radaelli E, Martin P, Signoretti S, Sullivan R, et al. Animal models of human prostate cancer: the consensus report of the New York meeting of the Mouse Models of Human Cancers Consortium Prostate Pathology Committee. Cancer Res 2013;73:2718–36.
23. Irshad S, Abate-Shen C. Modeling prostate cancer in mice: something old, something new, something premalignant, something metastatic. Cancer Metastasis Rev 2013;32:109–22.
24. Bianchi-Frias D, Hernandez SA, Coleman R, Wu H, Nelson PS. The landscape of somatic chromosomal copy number aberrations in GEM models of prostate carcinoma. Mol Cancer Res 2015;13:339–47.
25. Kim J, Eltoum IE, Roh M, Wang J, Abdulkadir SA. Interactions between cells with distinct mutations in c-MYC and Pten in prostate cancer. PLoS Genet 2009;5:e1000542.
26. Kim J, Roh M, Doubinskaia I, Algarroba GN, Eltoum IE, Abdulkadir SA. A mouse model of heterogeneous, c-MYC-initiated prostate cancer with loss of Pten and p53. Oncogene 2012;31:322–32.
27. Cho H, Herzka T, Zheng W, Qi J, Wilkinson JE, Bradner JE, et al. RapidCaP, a novel GEM model for metastatic prostate cancer analysis and therapy, reveals myc as a driver of Pten-mutant metastasis. Cancer Discov 2014;4:318–33.
28. McMullin RP, Mutton LN, Bieberich CJ. Hoxb13 regulatory elements mediate transgene expression during prostate organogenesis and carcinogenesis. Dev Dyn 2009;238:664–72.
29. Chen H, Mutton LN, Prins GS, Bieberich CJ. Distinct regulatory elements mediate the dynamic expression pattern of Nkx3.1. Dev Dyn 2005;234: 961–73.
30. Soriano P. Generalized lacZ expression with the ROSA26 Cre reporter strain. Nat Genet 1999;21:70–1.
31. Gossen M, Freundlieb S, Bender G, Muller G, Hillen W, Bujard H. Transcriptional activation by tetracyclines in mammalian cells. Science 1995;268:1766–9.
32. Lesche R, Groszer M, Gao J, Wang Y, Messing A, Sun H, et al. Cre/loxP-mediated inactivation of the murine Pten tumor suppressor gene. Genesis 2002;32:148–9.
33. Bethel CR, Faith D, Li X, Guan B, Hicks JL, Lan F, et al. Decreased NKX3.1 protein expression in focal prostatic atrophy, prostatic intraepithelial neoplasia and adenocarcinoma: association with Gleason score and chromosome 8p deletion. Cancer Res 2006;66:10683–90.
34. Copeland NG, Jenkins NA, Court DL. Recombineering: a powerful new tool for mouse functional genomics. Nat Rev Genet 2001;2:769–79.
35. Ellwood-Yen K, Graeber TG, Wongvipat J, Iruela-Arispe ML, Zhang J, Matusik R, et al. Myc-driven murine prostate cancer shares molecular features with human prostate tumors. Cancer Cell 2003;4:223–38.
36. Iwata T, Schultz D, Hicks J, Hubbard GK, Mutton LN, Lotan TL, et al. MYC overexpression induces prostatic intraepithelial neoplasia and loss of Nkx3.1 in mouse luminal epithelial cells. PLoS One 2010;5:e9427.
37. Wang S, Gao J, Lei Q, Rozengurt N, Pritchard C, Jiao J, et al. Prostate-specific deletion of the murine Pten tumor suppressor gene leads to metastatic prostate cancer. Cancer Cell 2003;4:209–21.
38. Gumuskaya B, Gurel B, Fedor H, Tan HL, Weier CA, Hicks JL, et al. Assessing the order of critical alterations in prostate cancer development and progression by IHC: further evidence that PTEN loss occurs subsequent to ERG gene fusion. Prostate Cancer Prostatic Dis 2013;16:209–15.
39. Aryee MJ, Liu W, Engelmann JC, Nuhn P, Gurel M, Haffner MC, et al. DNA methylation alterations exhibit intraindividual stability and interindividual heterogeneity in prostate cancer metastases. Sci Transl Med 2013;5: 169ra10.
40. Liu W, Laitinen S, Khan S, Vihinen M, Kowalski J, Yu G, et al. Copy number analysis indicates monoclonal origin of lethal metastatic prostate cancer. Nat Med 2009;15:559–65.
41. Haffner MC, Mosbruger T, Esopi DM, Fedor H, Heaphy CM, Walker DW, et al. Tracking the clonal origin of lethal prostate cancer. J Clin Invest 2013;123:6.
42. Prochownik EV, Li Y. The ever expanding role for c-Myc in promoting genomic instability. Cell Cycle 2007;6:1024–9.
43. Bassi C, Ho J, Srikumar T, Dowling RJ, Gorrini C, Miller SJ, et al. Nuclear PTEN controls DNA repair and sensitivity to genotoxic stress. Science 2013;341:395–9.
44. Clegg NJ, Couto SS, Wongvipat J, Hieronymus H, Carver BS, Taylor BS, et al. MYC cooperates with AKT in prostate tumorigenesis and alters sensitivity to mTOR inhibitors. PLoS One 2011;6:e17449.
45. Murphy DJ, Junttila MR, Pouyet L, Karnezis A, Shchors K, Bui DA, et al. Distinct thresholds govern Myc's biological output in vivo. Cancer Cell 2008;14:447–57.
46. Chen Z, Trotman LC, Shaffer D, Lin HK, Dotan ZA, Niki M, et al. Crucial role of p53-dependent cellular senescence in suppression of Pten-deficient tumorigenesis. Nature 2005;436:725–30.
47. Aparicio AM, Harzstark AL, Corn PG, Wen S, Araujo JC, Tu SM, et al. Platinum-based chemotherapy for variant castrate-resistant prostate cancer. Clin Cancer Res 2013;19:3621–30.
48. Mulholland DJ, Tran LM, Li Y, Cai H, Morim A, Wang S, et al. Cell autonomous role of PTEN in regulating castration-resistant prostate cancer growth. Cancer Cell 2011;19:792–804.
49. Carver BS, Chapinski C, Wongvipat J, Hieronymus H, Chen Y, Chandarlapaty S, et al. Reciprocal feedback regulation of PI3K and androgen receptor signaling in PTEN-deficient prostate cancer. Cancer Cell 2011;19:
575–86.
50. Takeda H, Nakamoto T, Kokontis J, Chodak GW, Chang C. Autoregulation of androgen receptor expression in rodent prostate: immunohistochemical and in situ hybridization analysis. Biochem Biophys Res Commun 1991;177:488–96.
51. Lin HK, Hu YC, Lee DK, Chang C. Regulation of androgen receptor signaling by PTEN (phosphatase and tensin homolog deleted on chromosome 10) tumor suppressor through distinct mechanisms in prostate cancer cells. Mol Endocrinol 2004;18:2409–23.
52. Lin HK, Hu YC, Yang L, Altuwaijri S, Chen YT, Kang HY, et al. Suppression versus induction of androgen receptor functions by the phosphatidylinositol 3-kinase/Akt pathway in prostate cancer LNCaP cells with different passage numbers. J Biol Chem 2003;278:50902–7.
53. Xu J, Lange EM, Lu L, Zheng SL, Wang Z, Thibodeau SN, et al. HOXB13 is a susceptibility gene for prostate cancer: results from the International

Consortium for Prostate Cancer Genetics (ICPCG). Hum Genet 2013;132: 5–14.
54. Ewing CM, Ray AM, Lange EM, Zuhlke KA, Robbins CM, Tembe WD, et al. Germline mutations in HOXB13 and prostate-cancer risk. N Engl J Med 2012;366:141–9.
55. Chen Z, Greenwood C, Isaacs WB, Foulkes WD, Sun J, Zheng SL, et al. The G84E mutation of HOXB13 is associated with increased risk for prostate cancer: results from the REDUCE trial. Carcinogenesis 2013;34:1260–4.
56. Wu X, Xu K, Zhang L, Deng Y, Lee P, Shapiro E, et al. Differentiation of the ductal epithelium and smooth muscle in the prostate gland are regulated by the Notch/PTEN-dependent mechanism. Dev Biol 2011; 356:337–49.
57. Mulholland DJ, Kobayashi N, Ruscetti M, Zhi A, Tran LM, Huang J, et al. Pten loss and RAS/MAPK activation cooperate to promote EMT and metastasis initiated from prostate cancer stem/progenitor cells. Cancer Res 2012;72:1878–89.
58. Aytes A, Mitrofanova A, Kinkade CW, Lefebvre C, Lei M, Phelan V, et al. ETV4 promotes metastasis in response to activation of PI3-kinase and Ras signaling in a mouse model of advanced prostate cancer. Proc Natl Acad Sci U S A 2013;110:E3506–15.